Neutral gas desorption and photoelectric emission from aluminum alloy vacuum chambers exposed to synchrotron radiation

O. Gröbner, A. G. Mathewson, P. Strubin, and E. Alge
Balzers AG, Balzers, Liechtenstein

R. Souchet
LURE, Orsay, France

(Received 9 June 1988; accepted 31 October 1988)

In an aluminum alloy vacuum chamber exposed to synchrotron radiation, the photoelectron currents produced were measured with the photons incident at low angles on the side wall and compared with normal incidence. The calculated photocurrents for normal incidence, using published values of the photoyield for oxidized Al, agree to within 15% with the measured values. Differences in the photocurrent dependence on photon spectrum at normal and glancing incidence were attributed to low-energy photons being totally reflected and hence producing no photoelectrons. It was established that, at glancing angles of incidence down to 11 mrad, a substantial—more than 20%—fraction of the synchrotron radiation is scattered around the vacuum chamber from the initial point of impact. During exposure to synchrotron radiation, the gases desorbed were H_2, CO, CO_2, and CH_4. The similar shapes of the dependence of the gas desorption and the photoelectron currents on the photon spectrum suggested that it is mainly the photoelectrons that are contributing to the desorption. It was estimated that electrons of 60 eV would produce the same gas desorption as synchrotron radiation with a critical energy of 3 keV.

I. INTRODUCTION

In the presence of beams in the Large Electron and Positron (LEP) storage ring, the synchrotron radiation induced neutral gas desorption from the Al alloy vacuum chamber walls will provide a large dynamic gas load. It has been proposed that desorption of neutral gas from surfaces exposed to photons takes place mainly via intermediate photoelectrons.[1–4] Nevertheless, direct desorption by energetic photons is not excluded, but since they occur simultaneously the two effects are difficult to separate. In the closed geometry of a vacuum chamber, secondary effects such as reflection and scattering of photons and the production of secondary electrons complicate the situation even further.

Synchrotron radiation produced in the magnetic field of the bending magnets and emitted within a narrow cone is incident on the wall of the vacuum chamber at typically 7 mrad (1 mrad = 0.0573°) grazing incidence. This region is the main source of reflected photons and of the primary photoelectrons. Due to the magnetic field, the photoelectron trajectories are curved and, in particular, the low-energy electrons are returned to the region of origin. The synchrotron radiation photons can be reflected and scattered across the vacuum chamber and hence may reach the whole surface.

To obtain a better knowledge of the importance of the scattered radiation and to make more reliable predictions of the expected gas load, LEP-type vacuum chambers were exposed to synchrotron radiation in a photon beam line of the DCI positron storage ring at the LURE Laboratory in Orsay, France.

The subject of this experiment has been to study as a function of the radiation spectrum: (i) the photoelectron production from Al alloy at normal incidence of the photons, (ii) the amount of synchrotron radiation scattered or reflected from the point of primary impact as a function of the angle of incidence, and (iii) the photoelectron production and the photon induced gas desorption at grazing incidence of the photons in the same test chamber.

II. EXPERIMENTAL DETAILS

A. Vacuum system

The experimental setup has been described fully in a previous publication[5] but for completeness, a brief outline will be given here.

Synchrotron radiation from a bending magnet of the DCI storage ring (3.82-m bending radius) is extracted from the machine through a tangential beam line. A set of collimator slits limits the angular divergence of the synchrotron radiation beam to 4.7 mrad in both the horizontal and the vertical direction. As a consequence of the vertical collimation the continuous photon spectrum is attenuated below ~6 eV. The photon beam, and thus the time of exposure of the test system, can be controlled by a radiation stopper. The test chamber, connected by a set of bellows at the downstream end of the system, could be pivoted in the horizontal plane in order to obtain the desired orientation between its axis and the photon beam. In the straight-through position, all photons were incident on the end face, while in an inclined position, the beam could be received at varying angles of incidence on the side wall of the test chamber.

The test chambers were pumped via a 72.5 l/s conductance by a combination of a 400 l/s ion pump and two Ti sublimation pumps. The pressure in the stainless-steel pumping system, which could be baked at 300 °C for 24 h, reached $\sim 7\times10^{-9}$ Pa while the aluminum test chamber, baked at 150 °C only, remained at typically 2×10^{-8} Pa. Pressure measurements were made by calibrated Bayard–Alpert gauges and with a quadrupole gas analyzer, which

 0734-2101/89/020223-07$01.00

could be calibrated *in situ* by injecting pure gases. Both data taking and analysis were performed by a specially developed microcomputer system.

B. Photoelectron probes

The first Al alloy test chamber, 3.6 m long, was equipped with two sets of five button electrodes to measure photoelectron currents. The layout of this chamber, showing its cross section and the mounting configuration of the electrodes, is given in Fig. 1. The section of the test chamber also shows the square cross-section size of the photon beam at the first and the second measuring positions, respectively. For symmetry reasons the electrodes were placed only on the top half of the chamber perimeter. The buttons were cut from an identical Al tube so that, when mounted, the shape of the electrodes matched exactly the contour of the test chamber and guaranteed identical surface properties. Furthermore, to avoid contributions to the measured photoelectron current from energetic photons, which may traverse the 5-mm-thick buttons and produce further photoelectrons , all probes were backed with 10-mm-thick copper disks and surrounded by a 1-mm-thick tantalum ring. At the downstream end of the test chamber a flat Al alloy electrode, again backed with 10-mm copper, was used to measure the total photoelectron current. All electrodes were mounted on UHV high-voltage feedthroughs and could be biased up to 1 kV, but all measurements of the photoelectron currents were carried out at a bias of -150 V at which a saturated current was obtained.

The second test chamber differed from the first insofar as the two sets of button electrodes were replaced by a single 0.2-m-long stainless-steel wire (1-mm diameter) which was suspended along the axis of the chamber. This electrode could collect photoelectrons produced on the wall of the chamber within its immediate vicinity. Since the collection efficiency of this electrode depends on the applied voltage, all measurements were made at the same bias of $+1$ kV.

C. Test chamber treatment

The test chambers were manufactured from extruded aluminum tubes. The material is a precipitation hardenable alloy of type ISO Al Mg Si 0.5. The chambers and the electron probes were cleaned by immersion in NaOH at a concentration of 45 g/l at 45 °C for ~2 min followed by rinsing in water and neutralization in a bath containing HNO_3 (50 vol %) and HF (3 vol %) at room temperature. The final rinsing in demineralized water was followed by drying at 80 °C in hot air.

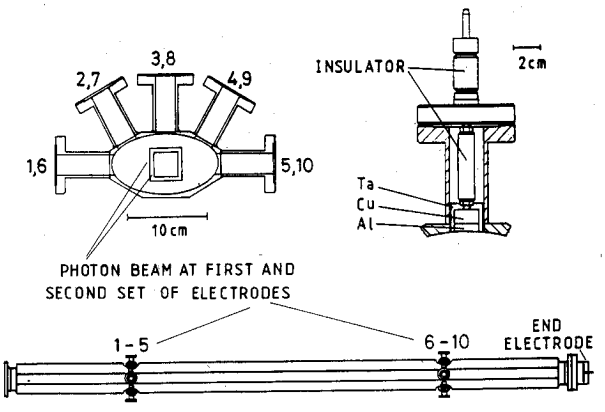

FIG. 1. Test vacuum chamber (total length 3.6 m) with two sets of button electrodes (1–5 and 6–10) mounted on high-voltage feedthroughs. The section of the photon beam at the position of the two sets of electrodes is shown.

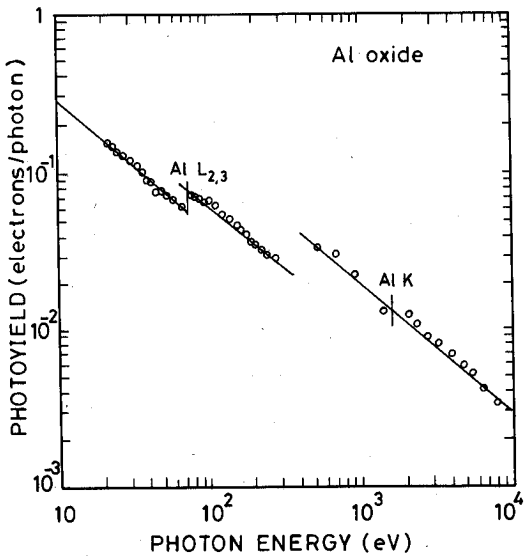

FIG. 2. Normal incidence photoelectric yield for oxidized aluminum as a function of the photon energy.

III. CALCULATION OF THE PHOTOCURRENT

The number of photons in the synchrotron radiation spectrum per mA of beam (di), per second (dt), and per eV ($d\epsilon$) is given by

$$\frac{d^3N}{di\,dt\,d\epsilon} = 6.95\times10^{13}\,\frac{\rho}{E^2}\int_y^\infty K_{5/3}(x)dx,$$

where E is the beam energy in GeV; ρ is the bending radius, for DCI 3.82 m; $y=\epsilon/\epsilon_c$; $K_{5/3}$ is a modified Bessel function of second kind of order $\frac{5}{3}$; ϵ is the photon energy in eV; and ϵ_c is the critical energy $=2.2\times10^3\,E^3/\rho$.

The total number of photoelectrons produced by the synchrotron radiation beam is obtained by integrating the product of the spectrum and the normal incidence photoelectric yield Y of Al oxide[6] shown in Fig. 2. For physical reasons, a lower integration limit of 10 eV was chosen, since below that energy the photoelectric yield is very low. (At the upper limit, 10 ϵ_c, the number of photons in the spectrum is negligible.) The measurements cover the beam energy range from 1.1 to 1.8 GeV, corresponding to a critical energy of the photon spectrum between 773 eV and 3.38 keV.

The photoyield Y was approximated by the following three expressions:

$$Y=1.60\,\epsilon^{-0.79},\quad 10<\epsilon<73\text{ eV},$$
$$Y=1.85\,\epsilon^{-0.75},\quad 73<\epsilon<400\text{ eV},$$
$$Y=5.71\,\epsilon^{-0.82},\quad 400<\epsilon<10\epsilon_c.$$

It must be remembered that the published photoyield measurements were made on bulk samples in vacuum which,

although not specifically mentioned in the publication, were most likely not baked. In addition, the measurements employed three different radiation sources to cover the range 25 eV–10 keV, i.e., most likely the samples were exposed to air between measurements. Furthermore, the authors stated that they did not attempt to prepare photocathodes of highest purity and cleanliness rather to use commercially available "high purity" (99%) samples dry machined and cleaned in Freon and ethanol.

The expression used to calculate the total number of photoelectrons produced by photons at perpendicular incidence, per mA of beam, per second, and per radian of beam orbit (da) is therefore

$$\frac{d^3N_e}{dt\,di\,da} = \frac{6.95\times10^{13}}{2\pi}\frac{\rho}{E^2}\int_{10}^{10\epsilon_c} Y(\epsilon)\int_y^{\infty} K_{5/3}(x)dx\,d\epsilon.$$

In the geometry chosen for our measurements, the test chamber receives photons from an arc of 4.7 mrad determined by the width of the horizontal collimator.

IV. RESULTS

A. Normal incidence photoelectron current

The normal incidence photoelectron currents were measured with the test chamber in the straight-through position and the entire photon beam incident on the end face electrode. With a bias of -150 V, a saturated current could be obtained at all beam energies. The results of these measurements are shown in Fig. 3. The full curve gives the calculated photocurrent. Of the two sets of experimental data, the first (before beam cleaning) refers to the initial measurement at the start of the exposure to synchrotron radiation, while the second set (after beam cleaning) has been taken after a prolonged exposure to synchrotron radiation at 1.1 GeV, with grazing incidence of 11 mrad on the side wall. As it will be discussed in the following section, the end face electrode had been exposed during this period to a substantial amount of radiation reflected from the side wall. As a consequence the photocurrent has decreased by $\sim 10\%$. In spite of this apparent dependence on the photon exposure the photoelectron current may be calculated to within better than 15% using the published photoyield data.

B. Grazing incidence photoelectron current and scattered radiation

The photoelectron currents due to scattered and reflected radiation could be studied by positioning the test chamber at different angles with respect to the synchrotron radiation beam. The angular positions used in this experiment were 11, 20, and 40 mrad. The positions of the test chamber, of the two sets of photoelectron probes and of the end face electrode with respect to the photon beam are shown in Fig. 4. Probes 1 and 6 lie in the horizontal plane and are, with the exception of probe 6 in the 20- and 40-mrad positions, directly illuminated by the photon beam. All other probes, including the end face electrode, are exposed to scattered photons only.

A typical result of a series of measurements at 11-mrad angle of incidence with the probes 1–5 is shown in Fig. 5. From this figure and from analysis of the other results it can be concluded that the directly illuminated probe always gives the largest current. The indirectly exposed probes show a nearly uniform photoelectron distribution, suggesting that the photons are diffusely reflected rather than specularly. Further evidence of this finding will be given when discussing the results from the end face electrode.

In Fig. 2 the height of the chamber directly illuminated

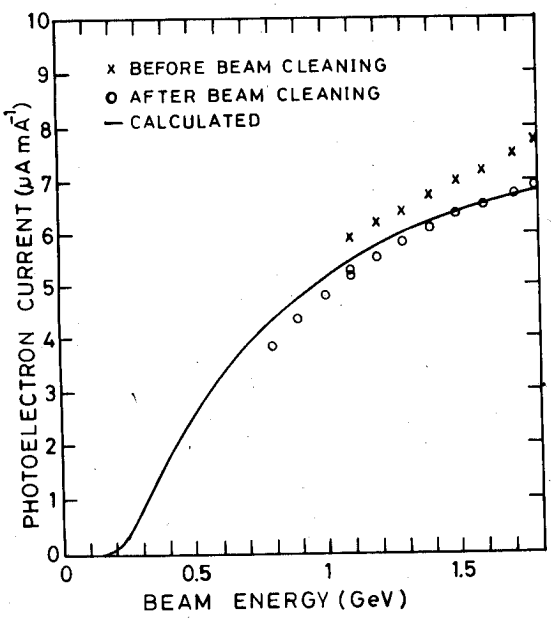

FIG. 3. Calculated and measured photoelectron current from the end face electrode as a function of the circulating beam energy before and after a period of beam cleaning.

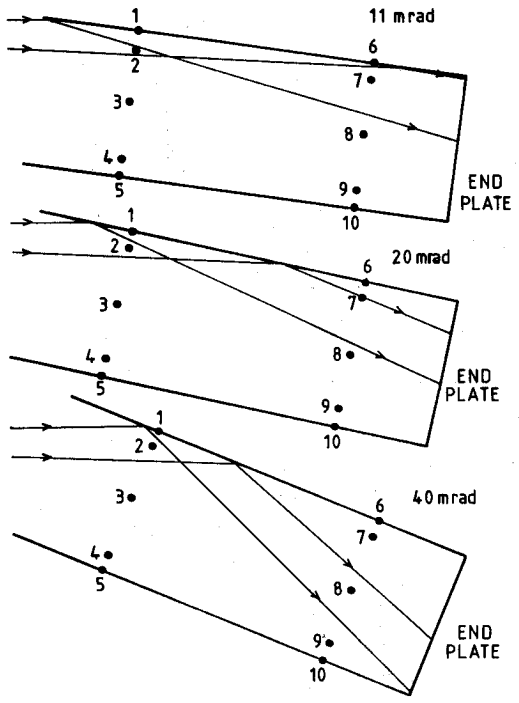

FIG. 4. Position of the button electrodes and of the end face electrode with respect to the photon beam at the angular positions 11, 20, and 40 mrad.

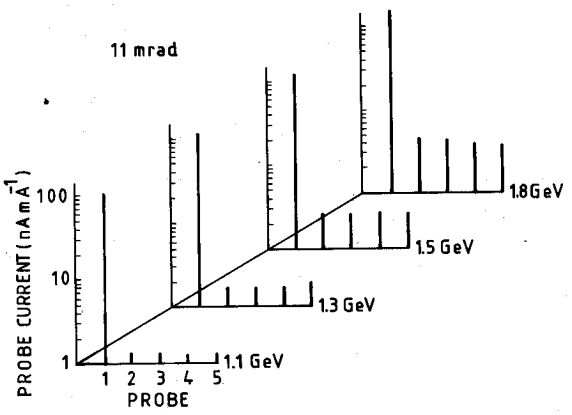

FIG. 5. Photoelectron current on the first set of button electrodes (1–5) at the 11-mrad position for different beam energies.

around probes 1 or 6 can be seen, hence the area can be calculated. From data as presented in Fig. 5, where the photocurrent from probe 1 is given and assuming a uniform photoelectron distribution over this directly illuminated area, the total photocurrent due to direct radiation can be calculated. For the rest of the chamber, taking an average probe photocurrent, the total photocurrent due to the scattered radiation can be calculated. This result is presented in Fig. 6, which gives, as a function of the beam energy, the ratio of the photocurrents for the indirectly and the directly exposed parts of the vacuum chamber perimeter. It can be seen that this ratio increases steeply with beam energy and exceeds 20% at the maximum energy of 1.8 GeV.

As the angle of incidence increases, the locally measured fraction of scattered radiation increases. In addition, a considerable number of photons appears to be deflected in the forward direction along the test chamber since probes 9 and 10 of the second set show a significantly enhanced signal at the 20-mrad position. It can be observed in Fig. 4 that in this configuration the wall in the vicinity of these probes is outside the directly illuminated zone.

C. Reflected synchrotron radiation incident on the end plate

The part of the photon beam scattered or reflected from the side wall of the vacuum chamber has been further studied by measuring the photoelectron current on the end face electrode. Independent of the orientation of the test chamber at 11, 20, or 40 mrad (see also Fig. 4), all of the specularly reflected part of the photon beam would hit the end electrode at practically perpendicular incidence. The measured photocurrent over the beam energy range from 1.1 to 1.8 GeV at 11-mrad incidence is shown in Fig. 7. For comparison, the calculated curve for perpendicular incidence of the primary photon beam has been included in this figure. As may be seen, only a small fraction of the photons reaches the end face electrode. Nevertheless, at 1.8 GeV this current is ~20% of that produced by the primary radiation.

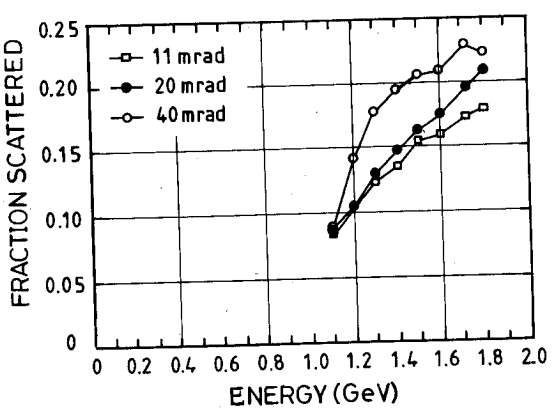

FIG. 6. Fraction of the total photoelectron current due to scattered photons measured on the first set of button electrodes for three angles of incidence.

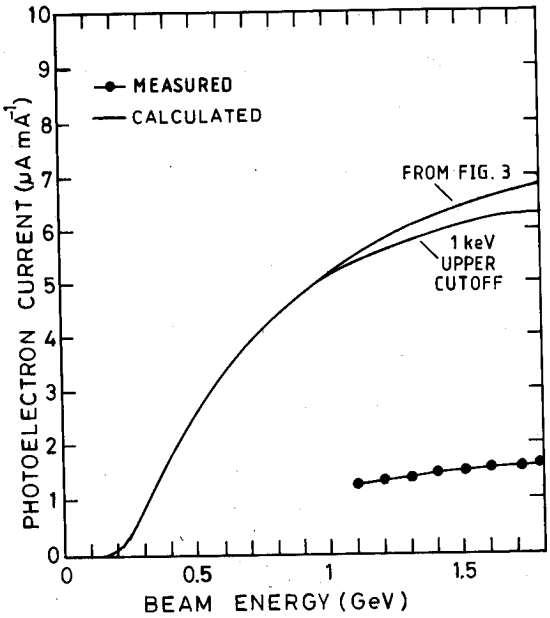

FIG. 7. Photoelectron current from the end face electrode due to photons reflected at 11-mrad grazing incidence on the side wall of the test chamber as a function of the circulating beam energy. For comparison the photoelectron current of Fig. 3 is shown as well as the current calculated by assuming that photons above an energy of 1 keV are not reflected on the side wall.

D. Photoelectron currents and photon induced gas desorption

The measurements referred to in this section have been made with the second test chamber, i.e., the chamber fitted with the central wire as photoelectron collector. During these experiments, the chamber was maintained at 11 mrad with respect to the photon beam direction and thus photons could strike the wall of the test chamber over a distance of ~3.2 m. The synchrotron radiation induced gas desorption and the photocurrent could be measured simultaneously as a function of the beam energy. For practical reasons and, in particular, to avoid any significant cleaning effect which would have affected the results of the desorption measurement, the test was done with low beam intensity and by opening the radiation stopper for the minimum time only.

The results of the total specific gas desorption and of the photoelectron current are shown in Figs. 8 and 9, respectively. In both figures, the ordinate has been normalized to the stored beam intensity in DCI. During exposure to synchro-

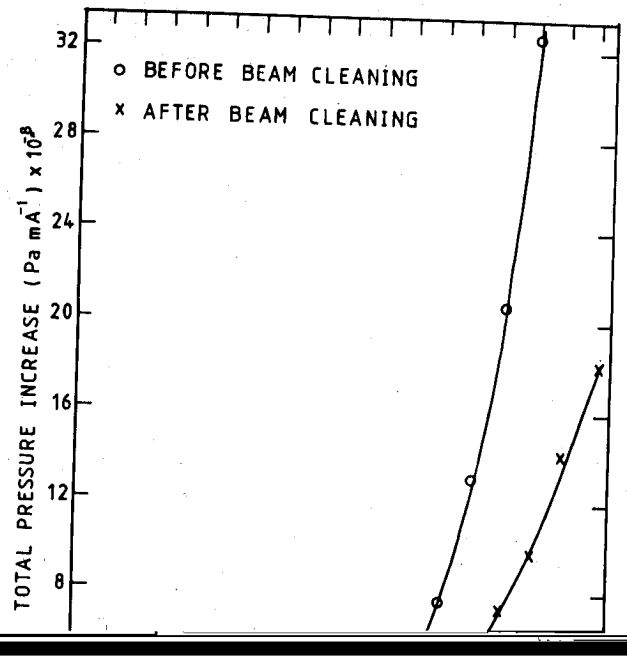

been plotted in Fig. 8. The total specific pressure rise and the photoelectron current collected with the wire electrode both follow a similar, steep rise with stored beam energy. Continued exposure to the synchrotron radiation cleans the vacuum chamber and results in a reduction of the specific pressure rise which is, however, more pronounced at higher beam energy. This effect can be noted by comparing in Fig. 8 the curves referring to the measurements before and after the beam cleaning period. This lasted ~ 11 h and during this time the test chamber accumulated a total photon dose of 1.3×10^{21} photons/linear m.

The photocurrent measured with the wire electrode in this configuration of grazing incidence (shown in Fig. 9) differs markedly from the results at normal incidence in Fig. 3. Whereas the latter shows a saturation of the photoelectron current at high photon energies, in agreement with the calculation, the curve in Fig. 9 has a steep, almost exponential growth. In order to understand the difference between these two cases, a model has been proposed which takes into ac-

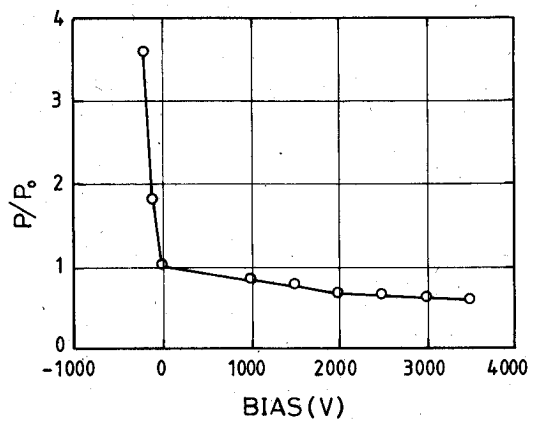

FIG. 10. Relative pressure variation observed in the test chamber with synchrotron radiation incident normally on the end face electrode as a function of the bias voltage on the electrode.

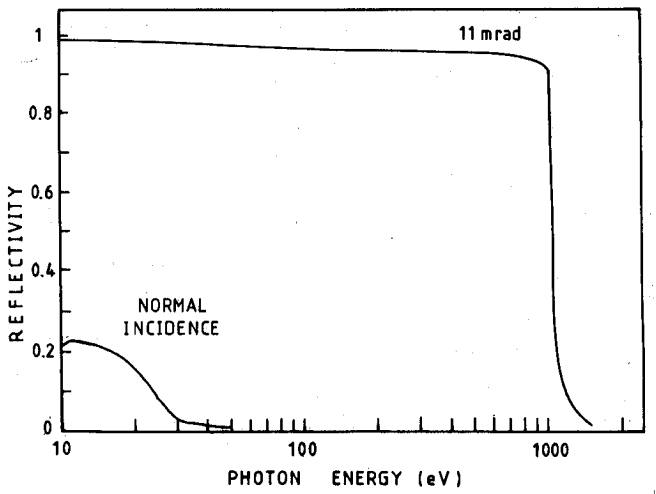

FIG. 11. Reflectivity of aluminum oxide at normal incidence (Ref. 9) and calculated values for 11-mrad grazing incidence as a function of the photon energy.

must now return to their origin and hence give rise to additional desorption from the electrode. In a situation where both surfaces have the same state of cleanliness, the pressure would not change. Since the results presented in Fig. 10 have been obtained after prolonged exposure of the end face electrode to the photon beam the decrease of the pressure is consistent with the described process and a relatively cleaner electrode surface. A very approximate, quantitative statement could be that under normal conditions, i.e., with no bias applied, at least one-half the global gas desorption is attributed to photoelectrons bombarding the surrounding vacuum chamber. This fact must be borne in mind not only when one attempts to measure the photon induced desorption from small samples mounted inside a larger test vessel but also in the design of a vacuum system which incorporates local synchrotron radiation absorbers.

V. DISCUSSIONS AND CONCLUSIONS

A. Photoelectron production

Using published data of the photoelectric yield for oxidized aluminum, the calculated photoelectron current at normal incidence agrees closely with measurements over a range of critical energies from 773 eV to 3.38 keV. During continued exposure to the synchrotron radiation the photocurrent has shown a tendency to decrease.

At grazing incidence of the synchrotron radiation the photoelectron currents from the two sets of button electrodes suggest an approximately uniform distribution of the scattered photons over the indirectly exposed part of the vacuum chamber perimeter. The photoelectrons due to this scattered and reflected radiation increase strongly with photon energy, i.e., with increasing critical energy of the photon spectrum. This may be seen in different form either in Fig. 6 or in Fig. 9.

The dependence of the photoelectron current at grazing incidence on the energy of the circulating beam, i.e., on the spectrum of the synchrotron radiation, differs significantly from the perpendicular incidence case. This difference may be explained, however, if one assumes that at grazing incidence a large fraction of the low-energy spectrum is reflected and hence that these photons contribute neither to the photoelectrons which are collected on the central wire electrode nor to the gas desorption. Introducing this assumption of high reflectivity up to a certain photon energy[7] into the previous photoelectron current calculation, yields good agreement with the experiment. Indeed, the data in Fig. 9 may be fitted if total reflection for photons up to $\sim$1.2–1.5 keV is assumed. Such an energy for grazing incidence reflection of photons[8] is not unrealistic as may be seen from Fig. 11. This curve shows high reflectivity up to $\sim$1 keV and has been calculated for 11-mrad grazing incidence on a flat surface using published values of the real and imaginary part of the refractive index for aluminum oxide.[9] The photons thus reflected on the wall of the vacuum chamber, hit in turn the end face electrode at nearly perpendicular incidence. The photoelectrons produced are shown in Fig. 7, but the signal observed is by a factor of 4 lower than could be expected. However, this discrepancy may easily be attributed to the fact that the photon beam is not perfectly specularly reflected, i.e., the wall of the vacuum chamber not perfectly smooth.

B. Photon induced gas desorption

The observation that significant photoelectron currents (several μA/mA of circulating beam) are measured in the test chamber and that the dependence of the pressure increase is very similar to that of the photoelectron production makes it tempting to attribute the predominant part of the gas desorption to the photoelectrons.[10]

From Figs. 8 and 9 it can be deduced that a photoelectron current of $\sim 6.6\ \mu\text{A mA}^{-1}\ \text{m}^{-1}$, which corresponds to a total of 19 μA mA^{-1} for 3.2-m length of the test vacuum chamber, produces a pressure increase of 3.2×10^{-7} Pa mA^{-1} at the beginning of the experiment, i.e., before any beam cleaning. Under the simplifying assumption that the dominant gas desorbed is CO, for which the pumping speed is 72.5 l s^{-1}, this pressure rise corresponds to a molecular desorption coefficient $\eta = 5\times10^{-2}$ molecules/photoelec-

tron. For comparison, Ref. 10 quotes η values for CO and CO_2 of 0.5 molecules/electron for 600-eV electrons incident on a 150 °C baked Al alloy sample. Therefore, and since it is known that the desorption yield increases approximately proportionally with the bombarding electron energy up to a maximum at ~600 eV,[11] the observed desorption coefficient would be consistent with electrons of 60 eV, a realistic value.

In spite of the limitation of the arguments presented which cannot conclusively prove that photoelectrons are the only cause of gas desorption by synchrotron radiation, it would nevertheless appear that direct photon desorption is at least of little practical importance. Hence, a knowledge of electron induced desorption yields (easy to measure in the laboratory) with a reliable calculation of the expected photoelectron production can provide valuable design parameters and be used to predict the behavior of a vacuum system exposed to synchrotron radiation.

ACKNOWLEDGMENTS

The authors wish to thank Professor Y. Petroff and Dr. P. Marin of the LURE Laboratory for their support of this work and for providing the necessary machine time on DCI. The experience of the DCI operations crew is also gratefully acknowledged and the very competent assistance provided by Mr. J. Michaut for the alignment of the experiment is much appreciated. Mr. C. Flament and Mr. D. Latorre are also thanked for their technical assistance.

[1]E. Garwin, Stanford Linear Accelerator Center, Memo, 1963.
[2]G. E. Fischer and R. A. Mack, in Proceedings of the 11th Annual Symposium of the American Vacuum Society, Chicago, 1964, p. 123.
[3]M. Bernardini and L. Malter, in Ref. 2, p. 130.
[4]T. Kobari and H. Halama, J. Vac. Sci. Technol. A **5**, 2355 (1987).
[5]O. Gröbner, A. G. Mathewson, R. Souchet, H. Störi, and P. Strubin, Vacuum **33**(7), 397 (1983).
[6]R. H. Day, P. Lee, E. B. Saloman, and D. J. Nagel, J. Appl. Phys. **52**, 6965 (1981).
[7]M. Kobayashi, CERN Internal Report No. LEP-VA/MK/sm, 1984.
[8]D. H. Bilderback and S. Hubbard, Nucl. Instrum. Methods **195**, 91 (1982).
[9]H.-J. Hagemann, W. Gudat, and C. Kunz, Deutsches Elektronen Synchroron (DESY), Hamburg, West Germany, Internal Report No. DESY SR-74/7, 1974.
[10]M.-H. Achard, R. Calder, and A. Mathewson, Vacuum **29**(2), 53 (1979).
[11]M.-H. Achard, CERN Internal Report No. CERN-ISR-VA/76-34, 1976.